Hindawi
Journal of Nanomaterials
Volume 2017, Article ID 4308294, 8 pages
https://doi.org/10.1155/2017/4308294

Research Article

Stoichiometry Calculation in $Ba_xSr_{1-x}TiO_3$ Solid Solution Thin Films, Prepared by RF Cosputtering, Using X-Ray Diffraction Peak Positions and Boltzmann Sigmoidal Modelling

J. Reséndiz-Muñoz,[1] J. L. Fernández-Muñoz,[2] M. A. Corona-Rivera,[1] M. Zapata-Torres,[2] A. Márquez-Herrera,[3] M. Meléndez-Lira,[4,5] F. Caballero-Briones,[6] F. Chale-Lara,[6] and O. Zelaya-Ángel[5]

[1] *COARA, Universidad Autónoma de San Luis Potosí, Carretera a Cedral Km 5+600, 78700 Matehuala, SLP, Mexico*
[2] *Instituto Politécnico Nacional, Laboratorio de Materiales Funcionales, CICATA Legaria, Legaria 694, Col. Irrigación, 11500 Ciudad de México, Mexico*
[3] *Universidad de Guanajuato, Campus Irapuato-Salamanca, Ex-Hacienda el Copal, Km. 9, Irapuato-Silao AP311, 36500 Irapuato, GTO, Mexico*
[4] *Instituto de Ingeniería y Tecnología, Departamento de Física y Matemáticas, Universidad Autónoma de Ciudad Juárez, Ciudad Juárez, CHIH, Mexico*
[5] *Departamento de Física, CINVESTAV-IPN, Av. Instituto Politécnico Nacional 2508, Gustavo A. Madero, San Pedro Zacatenco, 07360 Ciudad de México, Mexico*
[6] *Instituto Politécnico Nacional, Materiales y Tecnologías para Energía, Salud y Medioambiente (GESMAT), CICATA Altamira, Km 14.5, Carretera Tampico-Puerto Industrial Altamira, 89600 Altamira, TAMPS, Mexico*

Correspondence should be addressed to J. L. Fernández-Muñoz; jlfernandez@ipn.mx

Received 3 April 2017; Revised 23 May 2017; Accepted 30 May 2017; Published 9 August 2017

Academic Editor: Philip D. Rack

A novel procedure based on the use of the Boltzmann equation to model the x parameter, the film deposition rate, and the optical band gap of $Ba_xSr_{1-x}TiO_3$ thin films is proposed. The $Ba_xSr_{1-x}TiO_3$ films were prepared by RF cosputtering from $BaTiO_3$ and $SrTiO_3$ targets changing the power applied to each magnetron to obtain different Ba/Sr contents. The method to calculate x consisted of fitting the angular shift of (110), (111), and (211) diffraction peaks observed as the density of substitutional Ba^{2+} increases in the solid solution when the applied RF power increases, followed by a scale transformation from applied power to x parameter using the Boltzmann equation. The Ba/Sr ratio was obtained from X-ray energy dispersive spectroscopy; the comparison with the X-ray diffraction derived composition shows a remarkable coincidence while the discrepancies offer a valuable diagnosis on the sputtering flux and phase composition. The proposed method allows a quick setup of the RF cosputtering system to control film composition providing a versatile tool to optimization of the process.

1. Introduction

The $Ba_xSr_{1-x}TiO_3$ solid solution (BST-SS) is a ceramic material with a great potential to be used in dynamic random access memories (DRAM) and integrated optic devices. It is known that ferroelectric and optical properties of BST-SS are stoichiometry dependent, for example, the electrical resistance, hysteresis cycle, and resistive switching [1], extinction coefficient and refraction index [2], the relative dielectric constant, breakdown strength, and energy density of multifunctional fibers [3], and the remanent polarization [4]. BST-SS usually crystallizes in a cubic lattice changing its lattice parameter between a (Å) = 4.0577 and a (Å) = 3.936 associated with the extreme compositions: $BaTiO_3$ (BTO) and $SrTiO_3$ (STO) [ICCD, PDF International cards 00-075-0215 (BTO); 00-040-1500 (STO)]. The progressive Sr

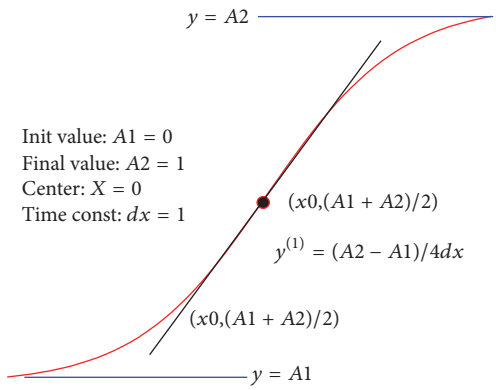

Figure 1: Scheme of a typical Boltzmann curve described by (1).

substitution in the $Ba_xSr_{1-x}TiO_3$ solid solution leads to a lattice contraction, reflected in the shift of Bragg angles, as reported in BST materials prepared by diverse techniques such as arc discharge [5], sol-gel [6–8] pulsed laser deposition [7], hydrothermal reaction [9], and chemical synthesis [10]. As much as both titanates are miscible in each other, the peak shift is linear and continuous between the extreme compositions; that is, it follows Vegard's law. However, the presence of the metastable tetragonal phase is possible due to the presence of oxygen vacancies [11, 12]. On the other hand, reactive sputtering modelling has been widely studied since the early work of Berg et al. [13]. Berg's and other models such as that developed by Strijckmans and Depla [14] take into account the nonlinearity inherent to the sputter deposition process involving reactive species. A general conclusion extracted from the models is that the hysteresis due to the change in the target (poisoned target) cannot be eliminated by the power fed to the RF system because the thickness of the compound film varies in proportion to the power and also depends on the reactive gas flux. The underlying mechanisms of the sputtering process using ceramic targets have been described since the early 1980s [15]. An accepted description of the process for ceramic targets is that the species are evaporated as individual atoms with different sputtering yields [16] causing an initial enrichment with the species of smaller yield, although a stationary point on the target composition compared with the sputtering flux is eventually reached. Usually oxygen is added to increase the control of film stoichiometry [11], although there is not yet an established procedure to control the sputtering process. Figure 1 depicts a scheme of the Boltzmann sigmoidal equation, where before and after of the exponential growth there are two zones of stabilization distinguished by a central turning point, $A1$, $A2$, and $(X0, (A1 + A2)/2)$, respectively. This function has also been used to describe other phenomena such as phase transition in smart gels [17], the relationship between reaction kinetics and its dynamic influence on viscosity in the chemorheology behavior of photopolymerizable acrylates [18], and the stem and rosebud growth in roses [19], among others.

Boltzmann's sigmoidal equation can be written as (1) when it is increasing and as (2) when it is decreasing.

$$y_{(x)} = y_f - \left[\frac{y_f - y_i}{\mathrm{A} + e^{(x-\mathrm{c})/\alpha}}\right], \quad (1)$$

$$y_{(x)} = y_i - \left[\frac{y_i - y_f}{\mathrm{A} + e^{(x-\mathrm{c})/\alpha}}\right], \quad (2)$$

where y_f and y_i are final values of the dependent variable, x the independent variable, c is the value of x at the inflection point, and α is a coefficient that describes the behavior of the slope of the process during the transition.

In the present contribution, a further development of the proposed Boltzmann modelling for BST-SS cosputtered films is presented in order to predict film properties such as film thickness and optical band gap, using as initial input the information extracted from X-ray diffractograms. The Boltzmann model is followed closely when the lattice parameter is plotted as a function of applied power.

2. Experimental Details

BST-SS films were prepared by RF magnetron sputtering in a system equipped with two magnetrons: $BaTiO_3$ (99.95%, SCI Engineered Materials Inc.) and $SrTiO_3$ (99.9%, SCI Engineered Materials Inc.). Targets were $2''$ diameter and $0.125''$ thick. Before film deposition, the sputtering chamber was evacuated to a base pressure around 1.2×10^{-3} Pa; then, an Ar flushing was done filling the chamber to a pressure of 3.9 Pa during 10 minutes. For the film deposition, an Ar + O_2 gas mixture was introduced into the chamber with an Ar/O_2 = 90/10 ratio at an initial pressure of 6.6 Pa to ignite the plasma and perform a target presputtering during 15 minutes. Thereafter, the working pressure was set at 3.9 Pa to carry out the deposition. Quartz substrates $1 \times 1\,\mathrm{cm}^2$ were successively rinsed with trichloroethylene, acetone, and ethanol before film deposit. A stainless-steel substrate holder was fixed at a distance of 8 cm from the magnetron in off-axis configuration. The substrate holder was rotated at 100 rpm for ensuring film uniformity; the substrate temperature was set at 549°C. The total applied RF-magnetron power was 120 watts, distributed between the two magnetrons as shown in Table 1, in order to produce $Ba_xSr_{1-x}TiO_3$ films with different *compositions*. The sputter deposit time for all of samples was 68 minutes.

Chemical composition was obtained by energy dispersive X-ray spectroscopy (EDS) employing a Jeol JSM-5300 electron microscope equipped with a Kevex Delta 1 spectrometer. The optical transmission spectra of the films were obtained in a Perkin-Elmer, Lambda 40 Spectrophotometer in the range of 250 to 800 nm. Film thicknesses were calculated from the transmittance spectra using the SCOUT software [20]. The X-ray diffractograms were acquired in a Phillips X'Pert diffractometer using CuKα = 1.54060 Å, in a 2 theta range 20–95° with a step size of 0.02° and step time 1 s in the grazing incidence geometry with an incidence angle 0.5°.

Table 1: RF power applied to $BaTiO_3$ and $SrTiO_3$ targets.

	Magnetron power (W)	
Sample	$BaTiO_3$	$SrTiO_3$
B0S120	0	120
B15S105	15	105
B30S90	30	90
B45S75	45	75
B60S60	60	60
B75S45	75	55
B90S30	90	30
B105S15	105	15
B120S0	120	0

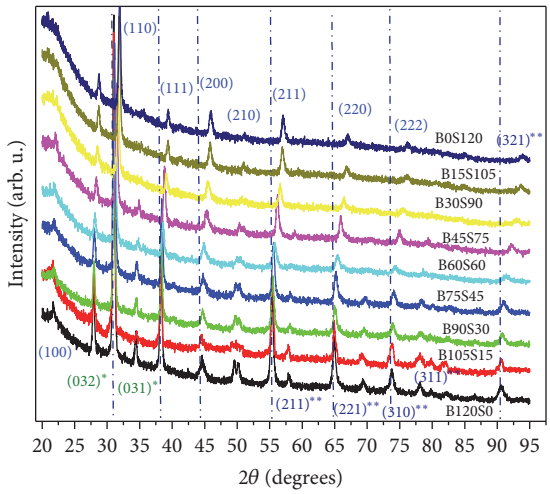

Figure 2: X-ray diffractograms for samples B120S0–B0S120. Peaks marked with "∗" correspond to the orthorhombic $Ba_{1.91}Sr_{0.09}TiO_4$ and those with "∗∗" to the tetragonal phase of BST-SS. Unmarked peaks correspond to the cubic phase.

3. Results and Discussion

Figure 2 presents the X-ray diffractograms of the BST-SS films described in Table 1. Diffraction peaks corresponding to (100), (111), (210), (211), (220), and (222) planes of the cubic BTO and STO phases were identified [21]. Diffraction peaks from (032) and (031) of the orthorhombic phase $Ba_{1.91}Sr_{0.09}TiO_4$ (marked with ∗) [22], planes of (221) and (321), planes of the BTO tetragonal phase, and those of (211), (221), (310), (311), and (321) planes (marked with ∗∗) of the BST-SS tetragonal phase [8, 18, 23] were also identified. As STO sputtering power increases a shift of the BTO cubic phase reflections at higher diffraction angles is observed, indicating a lattice contraction due to the higher Sr composition in the films. Figure 3 depicts the values of the diffraction angles for the (110) plane of the measured films versus applied power, fitted employing the Boltzmann sigmoidal equation. A similar analysis was carried out for the shift observed for the positions associated with (111) and (211) planes.

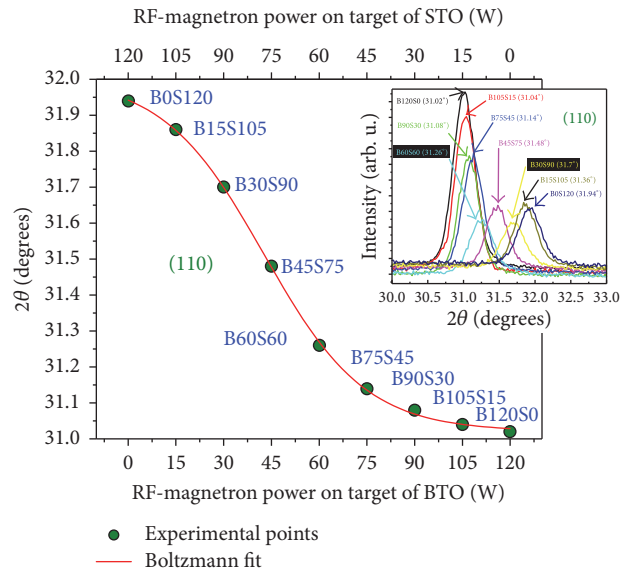

Figure 3: Boltzmann fitting to the peak position of the (110) plane of the prepared films as function of applied power.

The variables in (2) were assigned as follows: $y_{(x)}$ is $Ad_{(p)}$ representing the diffraction angle for the (110) plane; y_i is Ad_1 corresponding to the diffraction angle when the STO magnetron power is 120 W, y_f is Ad_2, the diffraction angle with a BTO magnetron power = 120 W, x is P which represents the magnetron power values; c is P_0, the middle value indicated to be $A = 1$, and α is ΔP which is the slope around P_0; thus (2) is rewritten as follows:

$$Ad\,(p) = Ad_1 - \left[\frac{Ad_1 - Ad_2}{1 + e^{(P-P_0)/\Delta P}}\right]. \tag{3}$$

The fitting values for Ad_1, Ad_2, P_0, ΔP, and R^2 for (110), (111), and (211) planes of the cubic phase are presented in Table 2.

Composition values x were obtained by considering that that peak shift follows Vegard's law with the extreme values corresponding to those of $SrTiO_3$ ($x = 0$) and $BaTiO_3$ ($x = 1$).

Figure 4 compares the XRD-derived stoichiometry evolution curve versus the magnetron power with the experimental composition measured by EDS, correspondingly fitted with Boltzmann's equation (Table 3). The Ba content was converted to x with the following expression:

$$\frac{\%\text{at Ba}}{\%\text{at Ba} + \%\text{at Sr}} = x. \tag{4}$$

Although the curves show a very close behavior, there is a separation in the middle part of the curve, that is, from BTO power = 30 W and from STO power = 15 W and a remarkable discontinuity between BTO magnetron power from 45 to 60 W. The inset in Figure 4 depicts the difference between the composition obtained from XRD (X_{XRD}) and that obtained from EDX measurements (X_{EDS}). To evaluate the discrepancy, in the inset the difference versus the power is plotted. The difference curve displays a bimodal increase when the power in each magnetron increases with a minimum value

Table 2: Fitting parameters for the peak positions versus the BTO magnetron power for (110), (111), and (211) peaks.

Peak	Ad_1 (degree)	Ad_2 (degree)	P_0 (W)	ΔP (W)	R^2
110	32.00 ± 0.01	31.02 ± 0.01	42.69 ± 0.65	15.94 ± 0.60	0.999
111	39.48 ± 0.03	38.29 ± 0.01	41.61 ± 1.4	15.73 ± 1.26	0.998
211	57.16 ± 0.06	55.36 ± 0.03	42.82 ± 1.75	15.52 ± 1.61	0.997

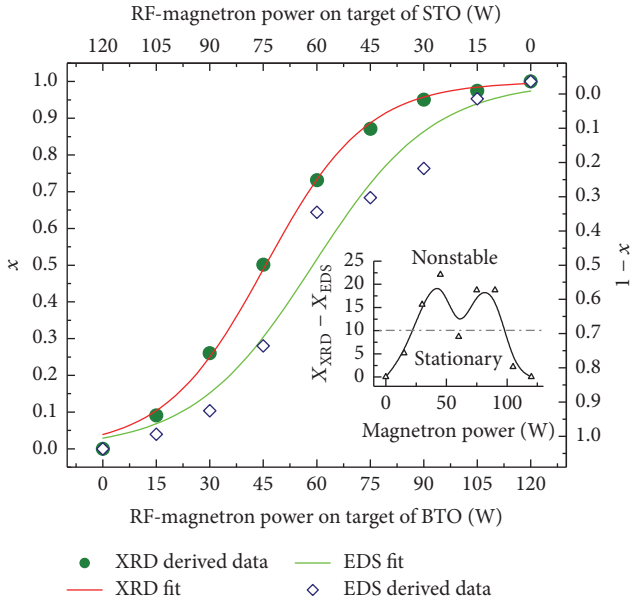

Figure 4: XRD and EDS derived composition versus power. The inset depicts the difference between XRD and EDS values.

Table 3: Boltzmann fit parameters for the EDS and XRD curves derived for x and $1 - x$ calculation.

Peak	x_1	x_2	P_0 (W)	ΔP (W)	R^2
110	0	100	45.69 ± 0.74	14.14 ± 0.65	0.997
111	0	100	43.81 ± 1.29	14.20 ± 1.15	0.992
211	0	100	46.74 ± 1.21	14.22 ± 1.07	0.993
EDS	0	100	58.93 ± 2.69	16.81 ± 2.40	0.973

at the point corresponding to the P_0 point in the Boltzmann fit. This point 59 W in the BTO magnetron corresponds to an x value around 0.5. Above $x > 0.5$ the tetragonal phase of $Ba_xSr_{1-x}TiO_3$ is reported [9, 14, 23], in accordance with the X-ray diffractograms in Figure 2.

The discrepancies observed between the EDS and XRD curves can be due to Ba-rich and Sr-rich composition volume zones in the film attributed to the variations in flux composition and Ba/Sr sputtering yields. When the power in a target, that is, the BTO target, begins to increase, decreasing power in STO target, an instability in the composition of the sputtered flux is expected because of the atomic masses in the system (Ba = 137.33 u, Sr = 87.62 u, Ti = 47.867 u, O_2 = 15.999 u, and Ar = 39.948 u), affecting not only the sputtering yield but also scattering between atoms of similar masses and the impinging ions. The Ba-rich and Sr-rich conditions are similar to those obtained in direct current arc discharge plasma process [5]. Composition also may be affected by changes in target erosion and total gas pressure during the sputtering process [13]. Additional discrepancies may be due to stress originated by the difference in size of Ba and Sr cations and to the different phases present in addition to the main one, interplanar spacing from XRD data is sensitive to these EDS measurements.

Table 4: Linear fit parameter for equation 5 using the diffraction peaks (110), (111), and (211).

Peak	A	B	R^2
(110)	$3.95 \pm 2E-4$	$0.00114 \pm 3E-6$	0.999
(111)	$3.95 \pm 1.5E-3$	$0.00111 \pm 2E-5$	0.998
(211)	$3.95 \pm 4E-4$	$0.00112 \pm 6E-6$	0.999

The values for the Boltzmann fit of the EDS curve are presented in Table 3 and compared with those from the XRD curves for (110), (111), and (211) diffraction planes. The values in (1), for the x_1 and x_2 parameters, were set at 0 and 1, respectively.

Figures 5(a) and 5(b) present the lattice parameter a (Å) calculated from diffraction peaks associated with (110), (111), and (211) planes of the prepared films versus the x parameters derived from XRD and EDS, respectively. Points were fitted with a straight line corresponding to Vegard's Law:

$$a\,(\text{Å}) = A + Bx, \tag{5}$$

where x is the molar fraction in $Ba_xSr_{1-x}TiO_3$ and "a" is the lattice parameter calculated from the XRD peaks (110), (111), and (211), respectively. Table 4 presents the A, B, and R^2 values, which indicate a linear relation of the composition of the cubic BST-SS with Vegard's law as observed in Figure 5(a).

The inset in Figure 5(a) presents the thickness of the studied samples as a function of the Ba composition obtained from XRD. The thickness reduction of the film B15S105 compared with that of pure SrTiO3 (B0S120) can be explained due to the mass difference, the sputtering yield, and scattering events. As the cosputtering process starts Ti ions would suffer additional scattering events due to the presence of Ba atoms affecting the film deposition rate. Also it is known that the sputtering yield of $SrTiO_3$ is smaller than that of $BaTiO_3$ [24]. It is worth emphasizing that, in this work, due to the employed deposition characteristics, the variation in the lattice parameter is due to the substitutional incorporation of Ba as its ionic radium is greater than that of Sr [1, 7]. The effect of differences in the thermal expansion coefficient (TEC) between substrate and BST-SS films is very important for epitaxial growth giving place to values of critical film thickness from 1 to ten nanometers [25]. Reported values of the TEC of BST-SS are close to those of $SrTiO_3$ and $BaTiO_3$,

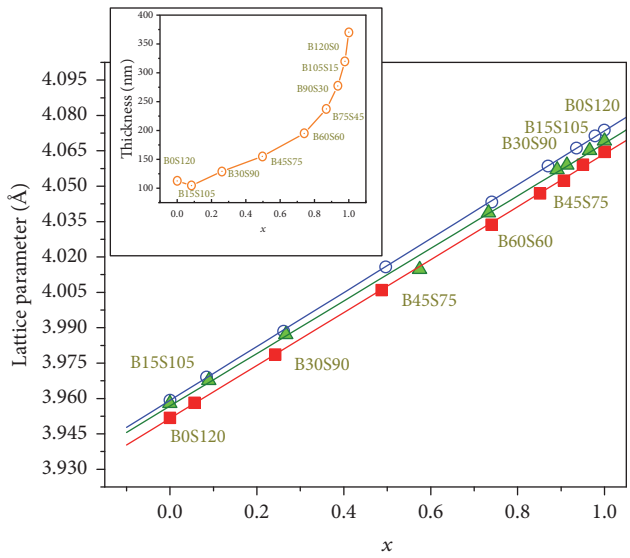

(a) Lattice parameter variation for (110), (111), and (211) planes versus the x parameter calculated from XRD data. The inset shows the thickness of the samples

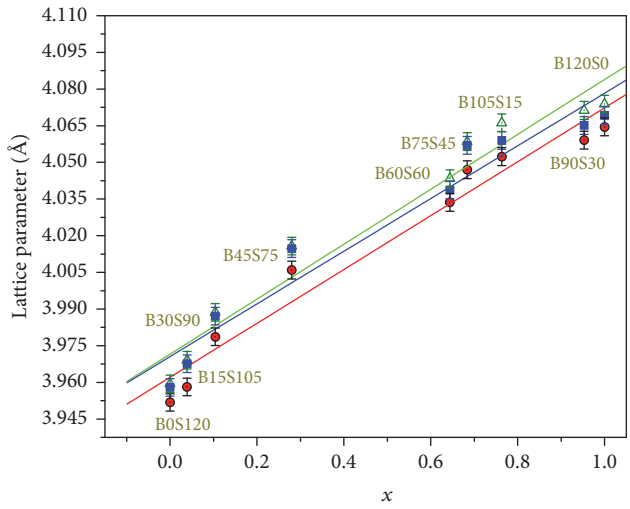

(b) Lattice parameter variation for (110), (111), and (211) planes versus the x parameter calculated from EDS data

Figure 5

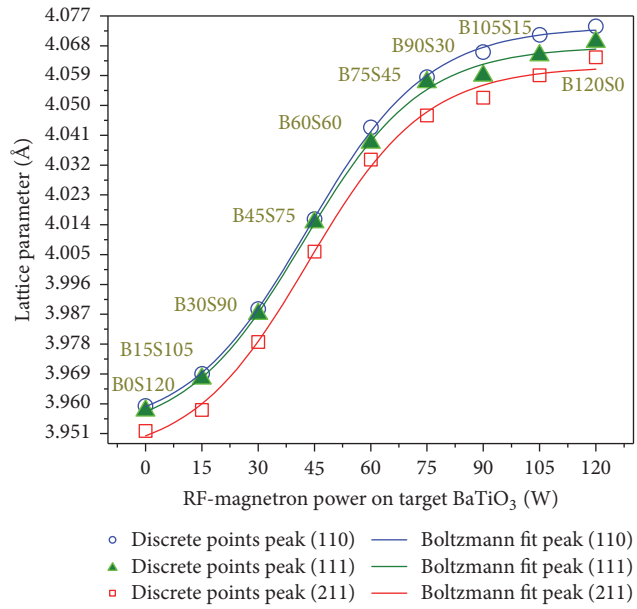

Figure 6: Lattice parameter variation for (110), (111), and (211) planes versus power. Solid lines correspond to Boltzmann fit.

$11 \times 10^{-6}\,^{\circ}\mathrm{C}^{-1}$ and $10.8 \times 10^{-6}\,^{\circ}\mathrm{C}^{-1}$, respectively [25–27]. In our case there is no an epitaxial growth not just because of the characteristics of the sputtering deposition technique but also due to the amorphous characteristics of the substrate. The reported value of the thermal expansion coefficient for quartz is $0.55 \times 10^{-6}\,^{\circ}\mathrm{C}^{-1}$ [28, 29]. Even when the difference between the TEC values of the films and the substrate is important, the close values of the TEC for the different compositions of the BST-SS allow affirming that if an effect due to the TEC difference would exist, it should affect in the same way to the whole set of samples, ruling out an effect on the observed trend of XRD peak positions.

Figure 5(b) shows the dependence of lattice parameter against composition values obtained from EDS. The greater scatter of data is expected due to the limitations of the EDS technique, mainly its lack of sensitivity to distinguish between the contribution from different crystallographic phases. Although Rietveld phase refinement is beyond the scope of the present contribution, it is a future task to elucidate the contribution of each phase in the cubic BST-SS.

The lattice parameter as a function of the RF-power is shown in Figure 6. The dependence follows a Boltzmann profile; a nonlinear behavior for a unique composition of Ba/Sr has been reported as a function of oxygen partial pressure and total gas pressure of the RF-magnetron sputtering process [11, 12].

The transmittance spectra of the deposited films are presented Figure 7(a) and analyzed according to Tauc model in Figure 7(b). In the transparent region (above the absorption edge) in the transmittance spectra, the number of interference maxima-minima reduces as the BTO sputtering power increases indicating a reduction in the film thickness, as will be discussed below. Correspondingly, the absorption edge shifts towards higher wavelength as is clearly observed in Figure 7(b).

By extrapolating the linear portion of the plot to $(\alpha h\nu)^2 = 0$, the band gap (E_g) values were calculated and presented in Figure 7(c) as a function of the composition parameter x. For the sake of fitting, both axes are inverted. The sigmoidal dependence of the band gap with composition is evident. The tendency in the band gap values for BST-SS agrees with those reported in literature [2, 6, 30, 31].

Figure 8 presents the evolution of deposition rate, calculated from the film thickness and the sputter time, with respect to (a) the RF-magnetron power and (b) the x parameter in the $Ba_xSr_{1-x}TiO_3$ solid solution. In Figure 8(a) a small decrement in the deposition rate is observed when the BTO target is turned on at the minimum power employed

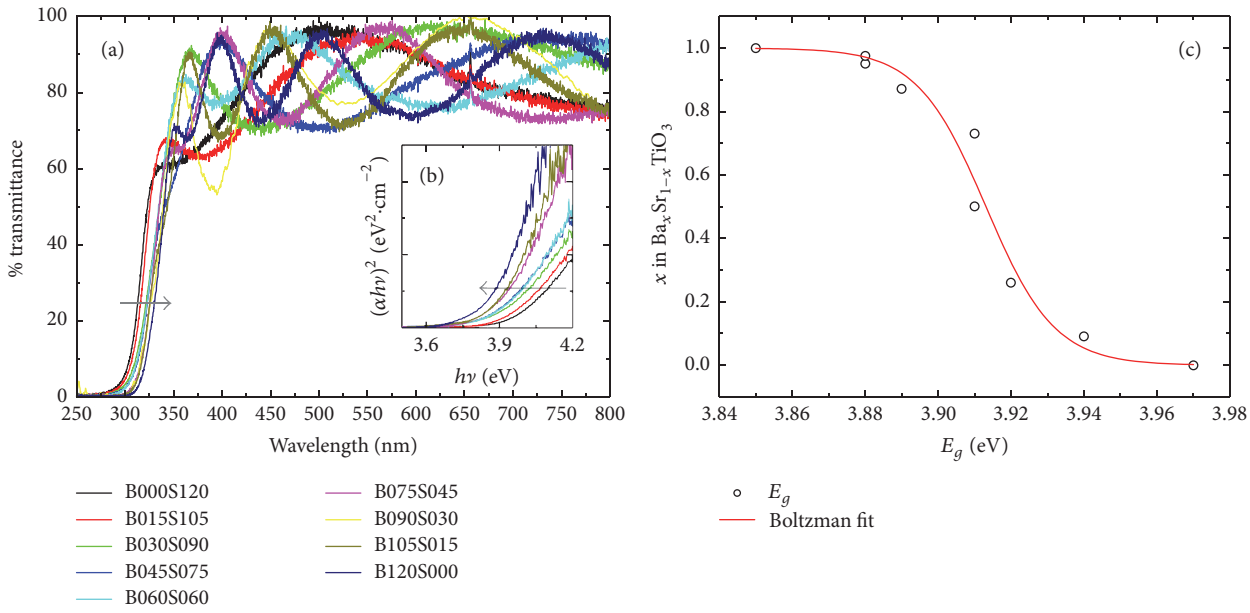

Figure 7: (a) Transmittance of the prepared films; (b) Tauc plots; (c) Boltzmann fit of the parameter x obtained by DRX against the optical band gap.

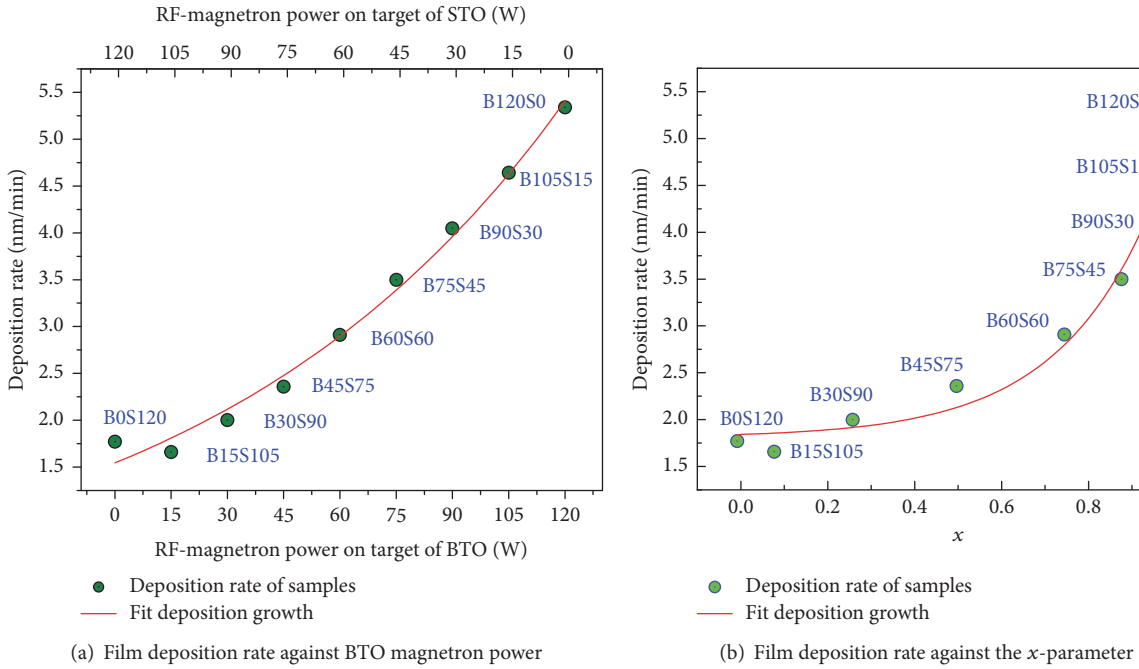

(a) Film deposition rate against BTO magnetron power

(b) Film deposition rate against the x-parameter

Figure 8

(105/15 power ratio STO/BTO). Thereafter the sputtering rate shows an exponential increase in the BTO magnetron power, fitted with the following expression:

$$Y = -0.037 + 1.582e^{P_{\mathrm{BTO}}(\mathrm{W})/97}. \quad (6)$$

Correspondingly, when compared with the x parameter, the deposition rate increases exponentially as follows:

$$Y = 1.807 + 0.033e^{x/22}. \quad (7)$$

In Figure 8(a) the relationship between deposition rate Ba/Sr and 120 W in both targets is approximately 3/1.

The calculations of the area under the Boltzmann curve fitted to DRX and EDS in Figure 4 show a relationship between Ba/Sr roughly 3/2 and 1/1 respectively; these results indicate a better relationship between the DRX Boltzmann fit and deposition rate compared with the relationship between EDS Boltzmann fit and deposition rate due to reasons previously explained. Therefore, the growing of X-parameter

is directly related to the increment in the magnitude of power on BTO. These facts allow us to conclude that the calculations of x-parameter based on DRX measurements are more accurate than those of EDS technique.

4. Conclusions

$Ba_xSr_{1-x}TiO_3$ (BST) films were grown on quartz substrates at 549°C by RF magnetron cosputtering from BTO and STO targets, using a total power of 120 W distributed between the two magnetrons. The films present a mixture of the cubic, orthorhombic, and tetragonal phases of BST. The Boltzmann fitting to the shift of diffraction peaks from the (110), (111), and (211) BST cubic phase planes as function of the applied RF-magnetron power allowed proposing a direct methodology to obtain the composition in $Ba_xSr_{1-x}TiO_3$ cubic solid solution. The "x" parameter calculated with the Boltzmann expression was compared with the x parameter obtained from the EDS measurements, and a close agreement was found. The lattice parameter variation versus power and the optical band gap versus the x parameter were adjusted with similar Boltzmann expressions. The film deposition rate as a function of power and x parameter follows an exponential growth behavior. The proposed method for estimation of the x parameter from simple X-ray diffraction analysis has been found useful for presetting the initial sputtering conditions to adjust x, film thicknesses, and optical band gap allowing a direct production of BST films with the adequate properties required for technological applications.

Disclosure

M. Meléndez-Lira is on sabbatical leave from Departamento de Fisica at Cinvestav-IPN.

Conflicts of Interest

The authors declare that there are no conflicts of interest regarding the publication of this paper.

Acknowledgments

J. Reséndiz-Muñoz acknowledges financial support from the Ph.D. Program in Engineering and Materials Science at UASLP. F. Caballero-Briones contribution was supported by SIP-IPN Multidisciplinary Project 20161804-043, 20170215, and by EDI and SIBE-IPN grants. M. Meléndez-Lira acknowledges partial financial support from CONACyT during the sabbatical leave at IIT-UACJ, and thanks are due to L. López and M. Guerrero for their technical assistance at CINVESTAV-IPN.

References

[1] A. Márquez-Herrera, E. Hernández-Rodríguez, M. P. Cruz et al., "Electrical properties of resistive switches based on Ba1-xSrxTiO3 thin films prepared by RF co-sputtering," *Revista Mexicana de Fisica*, vol. 56, no. 5, pp. 401–405, 2010.

[2] W. J. Leng, C. R. Yang, J. H. Zhang et al., "Structural and optical properties of Ba x Sr 1- x Ti O 3 thin films on indium tin oxide/quartz substrates prepared by radio-frequency magnetron sputtering," *Journal of Applied Physics*, vol. 99, no. 11, Article ID 114904, 2006.

[3] Y. Lin, Z. Zhou, and H. A. Sodano, "Barium titanate and barium strontium titanate coated carbon fibers for multifunctional structural capacitors," *Journal of Composite Materials*, vol. 47, no. 12, pp. 1527–1533, 2013.

[4] A. Zapata-Navarro, A. Márquez-Herrera, M. P. Cruz-Jáuregui, and M. L. Calzada, "Ferroelectric properties of barium strontium titanate thin films grown by RF co-sputtering," *Physica Status Solidi*, vol. 2, no. 10, pp. 3673–3676, 2005.

[5] S. Li, Y. Yao, Y. Jia, and Z. Cui, "Phase formation and microstructure of BaxSr 1-xTiO3 ceramics prepared by direct current arc discharge plasma process," *Materials Letters*, vol. 123, pp. 235–237, 2014.

[6] H. Y. Tian, H. L. W. Chan, C. L. Choy, and K. No, "The effects of composition gradients of Ba x Sr 1- x TiO 3 thin films on their microstructures, dielectric and optical properties," *Materials Science and Engineering: B*, vol. 103, no. 3, pp. 246–252, 2003.

[7] C. W. Beier, M. A. Cuevas, and R. L. Brutchey, "Low-temperature synthesis of solid-solution BaxSr 1-xTiO3 nanocrystals," *Journal of Materials Chemistry*, vol. 20, no. 24, pp. 5074–5079, 2010.

[8] S. Y. Kuo, W. Y. Liao, and W. F. Hsieh, "Structural ordering transition and repulsion of the giant LO-TO splitting in polycrystalline Ba x Sr 1- x TiO 3," *Physical Review B*, vol. 64, no. 22, Article ID 224103, 2001.

[9] H. Bouyanfif, J. Wolfman, M. El Marssi et al., "Combinatorial (Ba,Sr) TiO3 thin film growth: X-ray diffraction and Raman spectroscopy," *Journal of Applied Physics*, vol. 106, no. 3, Article ID 034108, 2009.

[10] S. Das, D. Liu, V. Janardhanam, C.-J. Choi, and Y.-B. Hahn, "Stoichiometry-controlled growth of Ba xSr 1-xTiO 3 thin films and their electrical behavior in heterojunction assemblies," *RSC Advances*, vol. 2, no. 27, pp. 10255–10261, 2012.

[11] F. Alema, A. Reinholz, and K. Pokhodnya, "Stoichiometry and phase purity control of radio frequency magnetron sputter deposited Ba0.45Sr0.55TiO3 thin films for tunable devices," *Journal of Applied Physics*, vol. 114, no. 17, Article ID 174104, 2013.

[12] S. Berg and T. Nyberg, "Fundamental understanding and modeling of reactive sputtering processes," *Thin Solid Films*, vol. 476, no. 2, pp. 215–230, 2005.

[13] S. Berg, H.-O. Blom, M. Moradi, and C. Nender, "Process modeling of reactive sputtering," *Journal of Vacuum Science Technology A: Vacuum, Surfaces, and Films*, vol. 7, article 1225, 1989.

[14] K. Strijckmans and D. Depla, "A time-dependent model for reactive sputter deposition," *Journal of Physics D: Applied Physics*, vol. 47, no. 23, Article ID 235302, 13 pages, 2014.

[15] C. J. McHargue, R. Kossowsky, and W. O. Hofer, *Structure-Property Relationships in Surface-Modified Ceramics*, Springer, Dordrecht, Netherlands, 1989.

[16] T. Nyberg, O. Kappertz, D. Rosen et al., in *Proceedings of the 48th Annual Technical Conference of Society of Vacuum Coaters*, Denver, Colo, USA, April 2005.

[17] A. L. Navarro-Verdugo, F. M. Goycoolea, G. Romero-Meléndez, I. Higuera-Ciapara, and W. Argüelles-Monal, "A modified Boltzmann sigmoidal model for the phase transition of smart gels," *Soft Matter*, vol. 7, no. 12, pp. 5847–5853, 2011.

[18] B. J. Love, F. P. Ruinet, and F. Teyssandier, "Chemorheology of photopolymerizable acrylates using a modified boltzmann sigmoidal model," *Journal of Polymer Science, Part B: Polymer Physics*, vol. 46, no. 21, pp. 2319–2325, 2008.

[19] J. J. Arévalo, J. E. Vélez, J. H. Camacho-Tamayo, J. J. Arévalo, and J. E. Vélez, "Uso eficiente del agua para el cultivo de rosa cv. Freedom bajo invernadero," *Revista Brasileira de Engenharia Agricola e Ambiental-Agriambi*, vol. 17, no. 8, 2013.

[20] W. Scout, "Theiss," in *Scout Thin Film Analysis Software Handbook*, Hard and Software, Aachen, Germany, code 1, page 10, 2012, http://www.mtheiss.com/.

[21] International Centre for Diffraction Data (ICDD), "PDF cards 00-040-1500 (STO); 00-075-0215 (BTO); 00-034-0411 (BST-SS with x=0.6)," (1982, 1997).

[22] American Ceramic Society, "Orthorhombic phase BST-SS PDF Card 130522 J," Kwestroo, Paping, 1959.

[23] H. Tang, Z. Zhou, and H. A. Sodano, "Large-scale synthesis of BaxSr1-xTiO3 nanowires with controlled stoichiometry," *Applied Physics Letters*, vol. 104, no. 14, Article ID 142905, 2014.

[24] J. Olejníek, Z. Hubička, P. Virostko et al., "Deposition of nanocrystalline and microcrystalline BaxSr 1-xTiO3 by means of pulse modulated low pressure plasma jet system," *Integrated Ferroelectrics*, vol. 81, pp. 227–237, 2006.

[25] Z.-G. Ban and S. P. Alpay, "Phase diagrams and dielectric response of epitaxial barium strontium titanate films: a theoretical analysis," *Journal of Applied Physics*, vol. 91, no. 11, pp. 9288–9296, 2002.

[26] J. A. Bland, "The thermal expansion of cubic Barium Titanate (BaTiO3) from 350∘C to 1050∘C," *Canadian Journal of Physics*, vol. 37, no. 4, pp. 417–421, 1959.

[27] F. W. Lytle, "X-ray diffractometry of low-temperature phase transformations in strontium titanate," *Journal of Applied Physics*, vol. 35, no. 7, pp. 2212–2215, 1964.

[28] C. Tsou, Y. S. Huang, H. C. Li, and T. H. Lai, "On the determination of thermal expansion coefficient of thermal oxide," in *Proceedings of the NSTI Nanotechnology Conf. and Trade Show (Nanotech '05)*, pp. 339–342, May 2005.

[29] T. F. Retajczyk Jr. and A. K. Sinha, "Elastic stiffness and thermal expansion coefficients of various refractory silicides and silicon nitride films," *Thin Solid Films*, vol. 70, no. 2, pp. 241–247, 1980.

[30] B. Panda, A. Dhar, G. D. Nigam, D. Bhattacharya, and S. K. Ray, "Optical properties of RF sputtered strontium substituted barium titanate thin films," *Thin Solid Films*, vol. 332, no. 1-2, pp. 46–49, 1998.

[31] P. Pasierb, S. Komornicki, and M. Radecka, "Structural and optical properties of Sr1-xBaxTiO3 thin films prepared by rf sputtering," *Thin Solid Films*, vol. 324, no. 1-2, pp. 134–140, 1998.